https://doi.org/10.15407/ujpe69.4.278

Y.M. AZHNIUK,[1] O.V. SELYSHCHEV,[2,3] YE.O. HAVRYLIUK,[2,3,4]
B.V. LOPUSHANSKA,[5] A. EHM,[2] V.V. LOPUSHANSKY,[1] A.V. GOMONNAI,[1,5]
I.P. STUDENYAK,[5] D.R.T. ZAHN[2,3]

[1] Institute of Electron Physics, Nat. Acad. Sci. Ukr.
(21, Universytetska Str., Uzhhorod 88017, Ukraine; e-mail: yu.azhniuk@gmail.com)
[2] Semiconductor Physics, Chemnitz University of Technology
(D-09107 Chemnitz, Germany)
[3] Center for Materials, Architectures and Integration of Nanomembranes (MAIN), Chemnitz University of Technology
(D-09107 Chemnitz, Germany)
[4] V. Lashkaryov Institute of Semiconductor Physics, Nat. Acad. Sci. Ukr.
(45, Prospect Nauky, Kyiv 03028, Ukraine)
[5] Uzhhorod National University
(3, Narodna Sq., Uzhhorod 88000, Ukraine)

GLUTATHIONE-CAPPED QUATERNARY Ag–(In,Ga)–S QUANTUM DOTS OBTAINED BY COLLOIDAL SYNTHESIS IN AQUEOUS SOLUTIONS

Ag–(In,Ga)–S quantum dots (QDs) were obtained by colloidal synthesis from aqueous solutions with different [In]/[Ga] precursor ratios in the presence of glutathione ligands under mild conditions. Size-selected fractions of the colloidal solutions were separated by the repeated centrifuging with addition of 2-propanol. The QD chemical composition determined by X-ray photoelectron spectroscopy is noticeably In-enriched with respect to the precursor ratio. The QD size estimated from the halfwidth of X-ray diffraction peaks for the non-fractioned colloidal solutions is about 2 nm. The synthesized QDs reveal a shift of the absorption edge and the photoluminescence (PL) peak maximum toward higher energies with decreasing the QD size. Experimentally measured Raman spectra of the Ag–(In,Ga)–S QDs are noticeably affected by size-related factors.

K e y w o r d s: colloidal synthesis, quantum dots, X-ray photoelectron spectroscopy, X-ray diffraction, optical absorption, photoluminescence, Raman spectroscopy.

1. Introduction

Within the last decade, ternary I–III–VI semiconductor quantum dots (QDs), in particular, Ag–In–S and Cu–In–S, emerged as low-toxicity alternatives to the well-studied II–VI QDs with a strong potential for applications in light-emitting diodes, solar cells, temperature sensors, photocatalysis, and biomedical experiments ([1–8] and numerous references therein). Ag–In–S and Cu–In–S QDs exhibit a clear size-dependent shift of the optical absorp-

C i t a t i o n: Azhniuk Y.M., Selyshchev O.V., Havryliuk Ye.O., Lopushanska B.V., Ehm A., Lopushansky V.V., Gomonnai A.V., Studenyak I.P., Zahn D.R.T. Glutathione-capped quaternary Ag–(In,Ga)–S quantum dots obtained by colloidal synthesis in aqueous solutions. *Ukr. J. Phys.* **69**, No. 4, 278 (2024). https://doi.org/10.15407/ujpe69.4.278.

Ц и т у в а н н я: Ажнюк Ю.М., Селищев О.В., Гаврилюк Є.О., Лопушанська Б.В., Ем А., Лопушанський В.В., Гомоннай А.В., Студеняк І.П., Цан Д.Р.Т. Вкриті глутатіоном чотирикомпонентні квантові точки Ag–(In,Ga)–S, отримані колоїдним синтезом у водних розчинах. *Укр. фіз. журн.* **69**, № 4, 278 (2024).

tion edge and intense size-tunable photoluminescence (PL) with a quantum yield up to 65–70 %, particularly increasing in intensity upon coating the QDs with a ZnS shell [9–12]. Based on the detailed studies of the PL size and temperature dependence, as well as its decay characteristics, a self-trapped exciton model was developed, explaining the PL mechanism for these ternary QDs [9, 13, 14].

Methods of colloidal synthesis of I–III–VI QDs can be broadly classified as organic phase and aqueous phase syntheses [8]. Organic synthesis generally involves the pyrolysis of precursors in the presence of hydrophobic solvents and capping agents/ligands at high temperatures under the inert atmosphere. It can be performed using the well-elaborated hot-injection, heating-up (non-injection), thermal decomposition, or solvothermal approaches and results in hydrophobic I–III–VI QDs. Water-soluble ternary QDs, which are particularly interesting for applications in biology and medicine, can be obtained from such hydrophobic QDs by ligand exchange [8]. Another route is a direct synthesis in an aqueous medium by arrested precipitation in the presence of mercaptoacetic (thioglycolic) acid (MAA), cysteine, glutathione (GSH), *etc.* [10, 11, 15]. These organic compounds provide strong binding to the QD surface by a mercapto group and prohibit the QD aggregation in the aqueous medium due to the electrostatic repulsion between deprotonated carboxylic anion groups [3, 11, 16]. The relative simplicity and the possibility of the direct use of the obtained QDs for biological applications are the advantages of water-based syntheses, although their luminescence efficiency is considered to be relatively lower due to the oxidation of the QD surface [17].

Further possibilities for tuning the I–III–VI QD optical properties can arise from a partial isovalent substitution of the constituent elements. In particular, the anion substitution $S \to Se$ can efficiently tune the bandgap of Cu–In–(S,Se) and Ag–In–(S,Se) QDs [18–20]. Partial replacement of $Ag \to Cu$ cations revealed the band bowing for (Cu,Ag)–In–S QDs [21, 22]. Even more complex multinary (Cu,Ag)–In–(S,Se) solid-solution QDs with simultaneous cation and anion substitution were reported [20]. In all these cases, the aqueous-based approach was applied for their synthesis.

Meanwhile, QDs of the Ag–(In,Ga)–S system, for which the replacement of the In^{3+} ion with another non-toxic trivalent Ga^{3+} ion leads to a significant bandgap widening, were obtained mostly by syntheses in organic media at elevated temperatures, namely by thermal decomposition of a single-source precursor [23, 24], a solvothermal process [25], a heating-up approach [26–29], hot injection [30, 31], and, in one case, using a hydrothermal process with cation exchange [32]. In this study, we report on Ag–(In,Ga)–S QDs with different In-to-Ga content ratios synthesised under mild conditions (below 100 °C) in aqueous solutions using glutathione (GSH) as a stabiliser. The QDs, fractionized for the size selection by repeated centrifuging with a poor solvent, are characterized by X-ray photoemission spectroscopy (XPS), X-ray diffraction (XRD), optical absorption, PL, and Raman spectroscopy.

2. Experimental

The colloidal synthesis of Ag–(In,Ga)–S QDs, including the end-point Ag–In–S and Ag–Ga–S ternary compounds, was based on an exchange reaction between Na_2S and a mixture of Ag(I), In(III), and Ga(III) thiolate complexes in the desired proportions with GSH in an aqueous solution (with addition of NH_4OH) at mild heating (93–98 °C) similarly to the earlier reports on obtaining brightly luminescent Ag–In–S [10, 11, 33, 34], Cu–In–S [35, 36], and Ag–Ga–S [37] QDs. We gave preference to GSH over MAA for the synthesis, since formerly [38] we found that GSH-capped Ag–In–S QDs exhibit a better stability upon long-term room-temperature storage than those stabilised by MAA. Gallium chloride was prepared in the form of 1.0 M aqueous solution by the reaction of metallic gallium (purity 99.9999%) with concentrated hydrochloric acid (35–37%, purity 99.98%). For the synthesis of QDs, we mixed 2.5 ml of deionized water with 2.4 ml of 0.5 M aqueous GSH solution and added 0.8 ml of a mixture of 1.0 M aqueous solutions of $InCl_3$ and $GaCl_3$ (in the appropriate proportion to provide a desired [In]/[Ga] ratio) with 0.05 ml of 0.2 M HNO_3. Then we added 1.0 ml of 0.2 M NH_4OH solution to the reaction mixture, followed by the addition of 2.0 ml of aqueous 0.1 M $AgNO_3$ solution and the rapid injection of 1.0 ml of 1.0 M aqueous Na_2S solution and adding 0.25 ml of 2.0 M aqueous solution of citric acid. Thus, all samples were prepared with a molar ratio of $[Ag]:[In+Ga]:[S] = 1:4:5$ in the reaction mixture, which earlier showed a considerable long-term stability for GSH-capped Ag–In–S

QDs [11, 38] and Ag–Ga–S QDs [37] obtained by a similar route. Depending on the [In]/[Ga] precursor ratio in the reaction mixture, the resulting solution acquired an intense red or dark red color. The above operations were performed under a constant magnetic stirring. Subsequently, the reaction mixture was heated in a water bath at 93–98 °C for 40 min.

Size separation of the synthesized QDs from the parental solution was performed by repeated centrifuging with addition, each time, of a new portion of a poor solvent (2-propanol C_3H_7OH), similarly to the procedure described earlier [10, 38, 39]. The initial portion of 1.6 ml C_3H_7OH was added to 4.0 ml of the QD solution obtained; then it was subjected to the centrifuging for 5 min at 4000 rpm to precipitate the first fraction, which was then separated and redissolved in deionized water. The multiple repeated procedure (addition of 0.4 ml of 2-propanol to the remaining supernatant, centrifugation, and redissolution of the precipitate) resulted in a series of fractions with decreasing average QD size, differing visually in color – from intense red or brownish (depending on the [In]/[Ga] ratio) to yellow and almost colorless for the fractions with the smallest QDs.

XPS measurements were performed using an ESCALAB 250Xi XPS Microprobe (Thermo Scientific) photoelectron spectrometer equipped with a monochromatized Al K_α X-ray source ($h\nu$ = = 1486.68 eV). The survey spectra were acquired at a bandpass energy of 200 eV. Data acquisition and spectra quantification were performed using Avantage software with adjusted Scofield sensitivity factors. For XRD studies, a Rigaku Smartlab operating with Cu K_α radiation was employed. The measurements were performed using the Bragg–Brentano and parallel–beam geometries for fractionised colloidal solutions of Ag–(In,Ga)–S QDs drop-casted onto a silicon substrate and dried at room temperature in a fume hood. Optical absorption spectra of the size-selected QD colloidal solutions were measured using a Cary 50 spectrophotometer (Varian) with a Xe pulse lamp source and dual Si diode detectors. For PL measurements, a Black Comet CXR-SR spectrometer (StellarNet) with diode excitation (λ_{exc} = = 390 nm) was employed. Micro-Raman measurements were performed using a LabRAM HR800 spectrometer equipped with a cooled CCD camera with the excitation by a $\lambda_{exc} = 488$ nm laser. For the micro-Raman studies, the aqueous solutions of the fractioned colloidal Ag–(In,Ga)–S QDs were drop-casted onto silicon substrates and dried at room temperature and ambient pressure. The spectral resolution was better than 2.5 cm^{-1}. All measurements were performed at room temperature.

Atomic percentage of Ag, In, Ga, and S in the synthesised Ag–(In,Ga)–S QDs determined from the XPS data. The subscript numbers in the QD sample notation correspond to the [In]/[Ga] molar ratio in the reaction mixture

Sample	Ag	In	Ga	S
Ag–($In_{75}Ga_{25}$)–S, fraction 1	11.4	24.0	5.2	55.1
Ag–($In_{75}Ga_{25}$)–S, fraction 2	11.0	24.8	4.8	59.4
Ag–($In_{50}Ga_{50}$)–S, fraction 1	18.9	19.9	8.0	53.2
Ag–($In_{50}Ga_{50}$)–S, fraction 2	9.9	14.4	8.1	67.6
Ag–($In_{25}Ga_{75}$)–S, fraction 1	11.4	13.0	19.0	56.6
Ag–($In_{25}Ga_{75}$)–S, fraction 2	12.3	13.3	16.0	58.4
Ag–Ga–S, fraction 1	23.9	–	26.3	49.8
Ag–Ga–S, fraction 2	20.0	–	30.3	49.7
Ag–Ga–S, fraction 3	6.5	–	36.2	57.3

3. Results and Discussion

The chemical compositions of the first three size-selected Ag–Ga–S QD fractions and the first two size-selected fractions of three solid-solution Ag–(In,Ga)–S QD samples were determined by means of XPS. Note that, for all samples, the presence of Na and Cl was detected, which were evidently contained in by-products of the exchange reaction not entirely removed from the solution. The concentrations of the elements of interest in the QDs determined from the XPS data are listed in Table.

As noted above, we used the molar precursor ratio [Ag] : [In+Ga] : [S] = 1 : 4 : 5 for the QD preparation, because it is known to provide long-term stability of QDs with the end-point compositions, as well as a high PL quantum yield [10, 11]. Such monovalent ion-deficient (or trivalent ion-rich) off-stoichiometry is generally considered preferable for obtaining the intense PL in I–III–VI QDs [30, 40]. It can be seen from Table that the correlation of the QD composition determined from the XPS data and the one in the reaction mixture is somewhat different for the ternary Ag–Ga–S and quaternary Ag–(In,Ga)–S QDs. For the solid-solution Ag–(In,Ga)–S QDs, the element content ratio [Ag] : [In+Ga] : [S] determined

from XPS correlates fairly well with the one in the reaction mixture. Besides, a trend of increasing concentration of sulphur with decreasing the QD size is revealed for the Ag–($In_{75}Ga_{25}$)–S and Ag–($In_{50}Ga_{50}$)–S QDs. For Ag–($In_{25}Ga_{75}$)–S QDs, this trend is less pronounced. Meanwhile, for Ag–Ga–S QDs, in spite of a considerable deficiency of silver and a strong excess of sulphur in the reaction mixture, the first fraction is nearly stoichiometric and the second one is slightly Ag-deficient without any over-stoichiometric sulphur content. For the third fraction with smaller QDs the trend toward silver deficiency and S excess is more noticeable, exhibiting a [Ag] : [Ga] : [S] ratio closer to the corresponding precursor ratio in the reaction mixture. The general trend of the increasing concentration of sulphur over the stoichiometric ratio with decreasing QD size can be explained by the fact that, in our case, the QDs are GSH-passivated, and sulphur atoms terminating the QD surface simultaneously belong to the GSH mercapto group. As for smaller QDs, the surface-to-volume ratio becomes higher, the amount of sulphur atoms forming the surface increases for smaller QDs noticeably above the stoichiometry.

With regard to the content of isovalent In and Ga atoms in the quaternary QDs, the XPS data enable two main conclusions to be made: (1) in all cases, the [In]/[Ga] ratio in the QDs prepared by the aqueous synthesis is noticeably higher than in the reaction mixture and (2) no marked dependence of the [In]/[Ga] ratio on the QD size is observed (at least for the first fractions).

Note that earlier XPS and EDX (energy-dispersive X-ray spectroscopy) studies of Ag–In–S QDs prepared by a similar method showed the actual [Ag]/[In] ratio to be somewhat different from the corresponding precursor concentration ratio, with the silver content being higher by factor of about 1.3 without any noticeable dependence on the QD size [11, 41]. As no gallium-containing QDs of this family prepared by this technique have been reported before, for the sake of comparison, one can check data for Ag–(In,Ga)–S QDs prepared by different colloidal techniques. In particular, for Ag–(In,Ga)–S QDs prepared by a solvothermal process [25], the ratio of [Ag] : [In+Ga] : [S] = 1 : 1 : 2 corresponding to stoichiometry as well as the correspondence of the [In]/[Ga] molar ratio in the QDs to that in the reaction mixture was confirmed by EDX measurements. Likewise, the stoichiometric composition and the desired [In]/[Ga] ratios were confirmed by EDX and XPS for Ag–(In,Ga)–S QDs obtained by a hydrothermal process with cation exchange [32]. For Ag-deficient non-stoichiometric Ag–(In,Ga)–S QDs prepared by the hot injection, the EDX-determined element content ratio also agrees with that in the reaction solution [31].

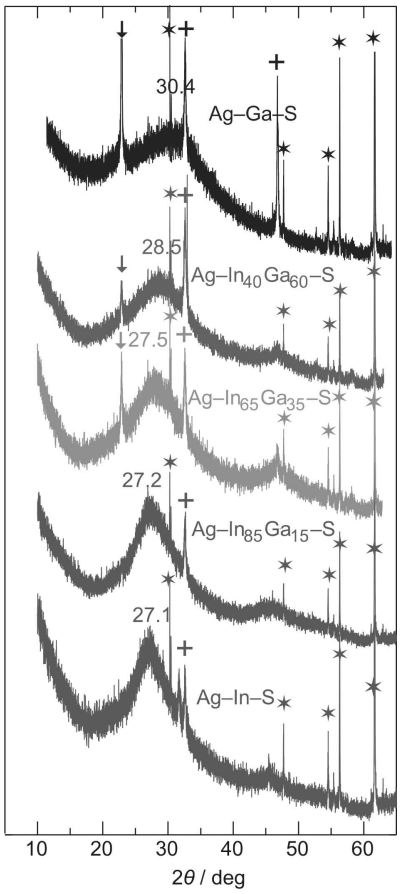

Fig. 1. X-ray diffractograms (Bragg–Brentano configuration) of Ag–(In,Ga)–S QDs prepared with a [Ag] : [In+Ga] : [S] precursor molar ratio of 1 : 4 : 5 drop-casted onto a silicon substrate. The [In]/[Ga] ratio in the quaternary QDs is indicated based on the XPS data, 85 : 15, 65 : 35, and 40 : 60 corresponding to the precursor ratio of 75 : 25, 50 : 50, and 25 : 75, respectively. Asterisks denote reflections from the silicon substrate, crosses correspond to the residual by-product NaCl peaks

XRD patterns of Ag–(In,Ga)–S QDs are shown in Fig. 1. Sharp peaks marked with asterisks are due to XRD from the crystalline silicon substrate (the most intense silicon peaks at 69.1° and 69.3° are not shown). Narrow peaks at 32.64° and 46.80°

marked by crosses (the latter is observed only for Ag–Ga–S QDs) are the most intense peaks in the rock salt diffraction pattern (JCPDS No. 5-0628) indicating the presence of residual NaCl formed due to the presence of sodium and chlorine ions in the reaction mixture. The sharp peak at 22.90° marked by an arrow (observed only for QDs with a noticeable amount of gallium) does not correlate with the known data for the tetragonal phase of $AgGaS_2$ (JCPDS No. 73-1233) [25, 42]. This peak cannot be related to Ga_2S_3 (JCPDS No. 84-1440) [43] or to Ag_2S (ICDD No. 00-024-0715), for which no peaks at these angles are known [44]. Most likely, this reflection is related to some contaminating agents, *e.g.* residual salts of synthesis by-products, which remained in a very small amount after the post-synthesis purification procedure, but, due to their high crystallinity, they were clearly manifested in the diffractograms.

It is known that XRD features from small nanocrystals, in particular, for Ag–In–S and Cu–In–S QDs of the same family obtained by colloidal chemistry methods, exhibit broad features [10, 11, 45–47] and, in our experiment (Fig. 1), such broad peaks are observed for each sample, gradually shifting from 27° to about 30° with In → Ga substitution. The gradual shift of the diffraction maximum indicates that the QDs in the ensemble are more likely to be solid-solution QDs with In and Ga atoms randomly distributed over the corresponding lattice sites rather than a co-existence of Ag–In–S and Ag–Ga–S phases. The position and compositional behavior of the observed maxima agree well with those reported for $AgIn_{1-x}Ga_xS_2$ QDs obtained by a solvothermal process [25]. As follows from the comparison with the data available for $AgInS_2$ [45–48], the observed peak for the end-point Ag–In–S QDs can be related to diffraction from (112) plane in the tetragonal (chalcopyrite) phase of $AgInS_2$ (JCPDS 00-025-1330 [49]). Aqueous colloidal tetragonal-like Ag–In–S QDs similar to our case exhibit this peak at around 26–27° [10, 11] in agreement with the peak of bulk chalcopyrite $AgInS_2$ at 26.67° (PDF 25-1330) [50]. Other atmospheric pressure phases, orthorhombic $AgInS_2$ (PDF 25-1328) [#48] and cubic spinel-type $AgIn_5S_8$ (PDF 25-1329) [50], show the most intense peaks at 28.38° and 27.32°, respectively. Under high pressure, tetragonal $AgInS_2$ either retains tetragonal structure with distortion, or, under pressure and heating, is transformed into spinel (partially starting at 0.04 GPa, 700 °C) [51], rocksalt-type (2.0 GPa, 400 °C) (no powder pattern data) [52] or rhombohedral α-$NaFeO_2$-type structure (4.0 GPa, 50 °C) with the major peak at 33.2° (PDF 22-1329) [44]. The Ag–(In,Ga)–S QD size for the non-fractioned colloidal solutions estimated from the width of the diffraction maximum using the well-known Scherrer equation is about 2 nm, which correlates with earlier data obtained for Ag–In–S QDs prepared by a similar method [10, 11, 39, 48]. Such value is obtained for all QD compositions except the end-point Ag–Ga–S QDs, for which the diffraction peak is noticeably broader. In our recent study [37], it was concluded from the position and width of the XRD peak near 30° that Ag–Ga–S QDs synthesized by this method possess a metastable (presumably, orthorhombic, rhombohedral, or rocksalt-type) structure rather than the conventional tetragonal chalcopyrite-type structure. The major (112) XRD peak of the latter is reported around 28° for the $AgGaS_2$ QDs prepared by the thermal decomposition [23], solvothermal process [25], or one-pot hot injection synthesis [31]. In view of the above-mentioned reports on Ag–In–S and Ag–Ga–S, from the gradual shift of the peak from 27.1° to about 28.5° for quaternary Ag–(In,Ga)–S QDs with In → Ga substitution, allows us to assign all studied quaternary QDs to the stable tetragonal-like structure; only for the end-point Ag–Ga–S, the QD structure becomes metastable (orthorhombic, rhombohedral, or rocksalt-type, see Ref. [37] for details). This difference in the nano-sized $AgGaS_2$ and $AgInS_2$ synthesized under the same conditions can be caused by the mismatch in ionic sizes. In^{3+} (0.80 Å) is closer to Ag^+ (1.14 Å) than the much smaller Ga^{3+} (0.62 Å), so that the $AgInS_2$ lattice relaxes more easily, whereas $AgGaS_2$ can be metastable with internal pressure. Note that chalcopyrite-type Ag–(In,Ga)–S QDs prepared by different routes in earlier studies [23, 25, 31] exhibit not only a similar gradual shift of the XRD peak with In → Ga substitution, but also a similar XRD peak halfwidth implying an average QD size of the same order.

Optical absorption spectra of a series of size-fractioned GSH-capped Ag–(In,Ga)–S QD solutions prepared with a [Ag] : [In] : [S] precursor molar ratio of 1 : 4 : 5 and equal In and Ga precursor molarity in the reaction mixture are shown in Fig. 2. Note that the absorption spectra of the end-point Ag–In–S and Ag–Ga–S QDs prepared by the same method with a

similar [Ag] : [In] : [S] precursor ratio were reported in our recent publications [37, 38]. Earlier studies of the optical properties of quaternary Ag–(In,Ga)–S QDs [23, 25, 26, 31, 32] revealed a clear dependence of the optical absorption edge on the QD composition, in particular, on the [In]/[Ga] ratio. However, no size dependence of the QD bandgap (either for different size-selected QD fractions, or for QDs of different sizes obtained under different reaction conditions) was reported. It can clearly be seen in Fig. 2 that, with increasing the fraction number, the absorption edge is significantly shifted toward higher energies, which is evidence of a decrease in the QD size. Contrary to the extensively studied II–VI QDs, for which (when the average QD size is below the exciton Bohr radius) distinct size-dependent maxima are observed in the optical absorption spectra enabling the QD size to be determined using the effective mass approximation [54], here we did not observe any confinement-related maxima. This is well known for Ag–In–S and Cu–In–S QDs and can be explained by the maxima being smeared due to the broadening of the absorption edge by defect states [10, 11]. The optical absorption spectra are plotted in Fig. 2 in the $(\alpha h\nu)^2$ versus $h\nu$ coordinates (where α is the absorption coefficient), appropriate for direct-bandgap semiconductors. This enables the bandgap value E_g to be estimated for each fraction by extrapolating the extended linear section to the intercept with the energy axis. The size behavior of thus evaluated E_g is shown as its dependence on the volumetric ratio of the 2-propanol to water in the QD solution at the corresponding fractioning stage, which is a more informative characteristic of the process than the mere fraction number. It is worth to note that, as follows from the XPS data, in this case the QDs in different fractions can differ not only in the average size, but also in the QD composition, and both of the factors contribute to the absorption edge shift with increasing fraction number.

Similarly to earlier observations for Ag–In–S QDs obtained by a similar approach [10, 11, 38], in our case (Fig. 3) for different Ag–(In,Ga)–S QD compositions the spectral position of the PL maximum shifts toward higher energies with increasing fraction number (decreasing QD size). A size-dependent PL maximum shift was also reported for $AgIn_{1-x}Ga_xS_2$ QDs synthesized by the thermal decomposition of a single-source precursor [23]. However, it can clearly be seen from Fig. 3 that the PL maximum shift for all

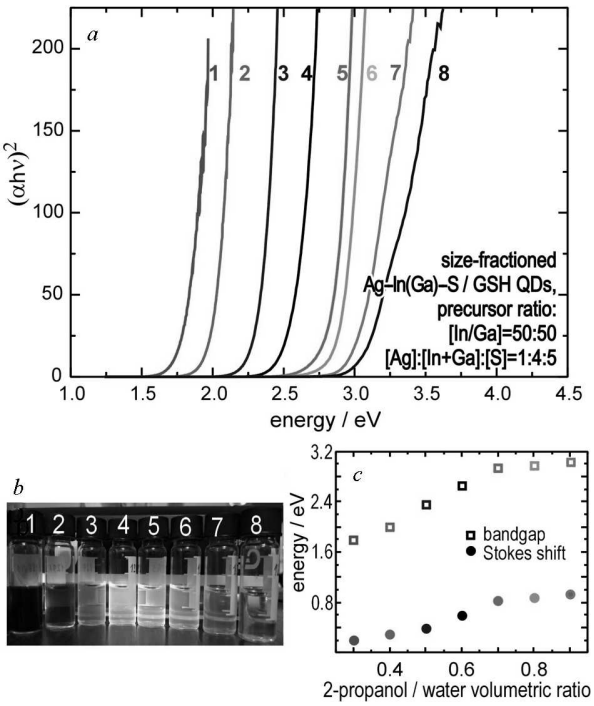

Fig. 2. Optical absorption spectra of a series of size-fractioned non-stoichiometric GSH-capped Ag–(In,Ga)–S QD solutions prepared with a [Ag] : [In] : [S] precursor molar ratio of 1 : 4 : 5 and a [In] : [Ga] precursor molar ratio of 1 : 1 (*a*), a photo of the size-fractioned Ag–(In,Ga)–S QD solutions under UV illumination (*b*), and dependence of the QD optical bandgap and Stokes shift on the volumetric ratio of the 2-propanol to water in the colloidal QD solution corresponding to the precipitated fraction (*c*)

compositional series is much smaller than that of the absorption edge. The Stokes shift (the energy difference between the optical bandgap and the PL maximum) strongly increases with decreasing QD size (see Fig. 2). A similar behavior was previously observed for Ag–In–S QDs and can be explained within the concept of the self-trapped exciton (STE) model by a larger number of phonons for smaller QDs emitted prior to the photon emission [11]. According to the STE model, one of the photogenerated carriers is localized at a certain QD lattice site, thereby resulting in a lattice distortion and strong electron-phonon interaction, due to which the broadband PL in I–III–VI QDs is treated as a series of phonon replicas of the pure excitonic (no-phonon) emission line [13, 55]. The Stokes shift is proportional to the Huang–Rhys factor S being the average number of phonons emitted prior to the PL event [39]. Frequencies of the

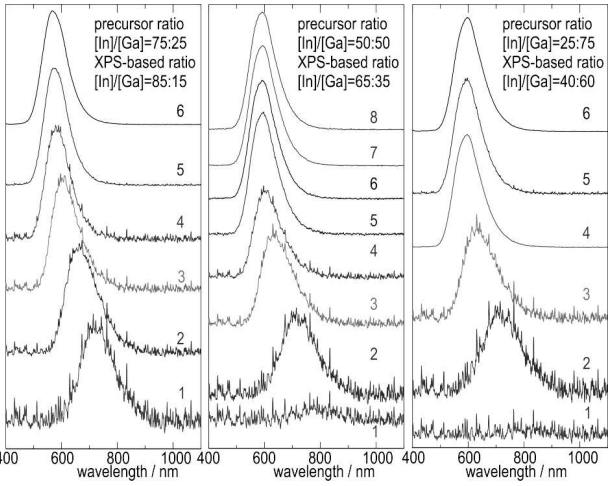

Fig. 3. PL spectra of series of size-fractioned non-stoichiometric GSH-capped Ag–(In,Ga)–S QD solutions prepared with [Ag] : [In] : [S] precursor molar ratio of 1 : 4 : 5 and three different [In] : [Ga] precursor molar ratios in the reaction mixture: 75 : 25 (*a*), 50 : 50 (*b*), and 25 : 75 (*c*). The corresponding XPS-estimated [In] : [Ga] ratios in the QDs are indicated in the figure. Size-selected fraction numbers are shown at each curve

most intense phonon maxima in the Raman spectra of the Ag–(In,Ga)–S QDs are near 300–350 cm^{-1} (37.5–44 meV), therefore S can be estimated to be from about 8–10 for the largest QDs (depending on the compositional series) to about 25 for the smallest ones (see Fig. 2). This corresponds to a much faster relaxation of the excitation energy for the smallest QDs in comparison to that of the bigger ones. As the GSH ligands on the QD surface may act as a "collective" trap for photogenerated holes [11], this agrees well with the higher surface-to-volume ratio for the smaller QDs.

The STE model explains the size-independent PL bandwidth observed for Ag–(In,Ga)–S QDs in Fig. 3 as well as in an earlier study [23]. Meanwhile, for Ag–In–S and Cu–In–S QDs, it is also well supported by the temperature-dependent PL behavior and PL decay data [13, 14, 55] while, for Ag–(In,Ga)–S QDs, no such data are available. Evidently, a conclusion on the applicability of the STE model for gallium-containing I–II–VI QDs requires more detailed studies.

As Ag–In–S QDs have been investigated far more extensively than Ag–Ga–S and the solid-solution QDs, it is not surprising that Raman data for the Ag–(In,Ga)–S QD system are available solely for the end-point Ag–In–S [21, 39, 41, 46, 56–58]. It should be noted that, in most cases, the analysis is encumbered by rather low signal-to-noise ratios and strong luminescence backgrounds. In our case for each composition we used the first size-selected fraction with the biggest QDs, for which the broadband PL peak maximum energy is the lowest (see Fig. 3), noticeably below the energy corresponding to the Raman excitation wavelength (488 nm). Still, for many samples, the PL background in the Raman measurements was quite intense. In order to quench the PL, we, similarly to earlier studies [21, 41], added to the colloidal solutions a small amount of methyl viologen that almost completely quenched the intense broadband PL of the QDs (except for the sample with Ag–Ga–S QDs, for which the first fraction exhibits no PL). Raman peaks of methyl viologen are revealed mostly at higher frequencies while its features in the range of interest are known to be narrow and relatively weak [21]. Besides, a comparison of the Raman spectra of Ag–In–S QDs measured with (Fig. 4) and without the addition of methyl viologen [39] did not reveal noticeable differences.

Raman spectra of the Ag–(In,Ga)–S QDs shown in Fig. 4 consist of a series of quite broad, mostly overlapping bands, which in fact exhibit only a slight compositional variation. In recent studies devoted to the Raman scattering of Ag–In–S QDs, the spectra were discussed based on symmetry analysis [41] or assignment of peaks to the vibrations of particular bonds in the nanoparticle structure [21, 38]. In all cases, the observed first-order spectra were approximated by a superposition of overlapping vibrational peaks, their number ranging from 4 [38] up to 10 [41]. Interestingly, Raman scattering in Ag–In–S QDs is studied much more widely [21, 34, 38, 39, 41, 46, 57, 59] than in bulk $AgInS_2$ crystals, for which, to our knowledge, the only experimental Raman data currently available refer to unpolarized spectra of polycrystalline $AgInS_2$ [60].

A separate study including Raman spectroscopy was devoted to solid-solution (Ag,Cu)–In–S QDs [21]. Note that the intense Raman features in the range of 280–350 cm^{-1}, including the contribution from the most intense A_1 symmetry mode typical of both Ag–In–S and Cu–In–S QDs [21, 41] did not reveal noticeable compositional variation. Meanwhile, for less pronounced maxima in the range of 175–255 cm^{-1}, a clear gradual shift with Ag→Cu substitution was

observed, showing a typical one-mode behavior [21] and thereby confirming the assignment of the band at 175 cm^{-1} to Ag–S bond vibrations [38]. On the contrary, the substitution of S by Se in Ag–In–(S,Se) and Cu–In–(S,Se) solid-solution QDs was clearly revealed in the Raman spectra by the appearance of sulphur-related and selenium-related features in different spectral ranges characteristic for a two-mode compositional behaviour [20].

In our case of solid-solution Ag–(In,Ga)–S QDs, we anticipated that substitution of indium in the QD lattice by lighter gallium atoms will result in a more pronounced contribution to the higher-frequency part of the spectrum. The most intense peak of the $AgGaS_2$ phonon spectrum is the A_1 symmetry vibration with a maximum near 290–295 cm^{-1} [61, 62]. Meanwhile, higher-frequency features, even though extending up to 390 cm^{-1}, exhibit much lower intensity [62]. Even though for bulk tetragonal $AgInS_2$ crystals, to our knowledge, only scarce experimental Raman data are available [60] and estimations predict an A_1 symmetry vibration frequency of 282 cm^{-1} [61], experimentally for stoichiometric and non-stoichiometric Ag–In–S QDs, the most intense Raman maxima are revealed at 290–300 cm^{-1} [21, 39, 41, 46, 57], which is in the same range that is expected for the Ag–Ga–S QDs. Although, based on theoretical predictions, one should anticipate compositional transformations of the Raman spectra of the Ag–(In,Ga)–S QDs with In→Ga substitution, we practically do not observe them experimentally and this agrees with the available experimental data for the end-point compounds. This is a notable difference of the materials under investigation from related solid-solution (Ag,Cu)–In–S QDs, for which Raman spectroscopy clearly confirms their quaternary composition [21] and even more from II–VI nanocrystals, for which Raman spectroscopy is known to be a very sensitive tool to evaluate the chemical composition of solid-solution QDs [63].

An important issue, which should be taken into account while analyzing the Ag–(In,Ga)–S QD Raman spectra, is their ultrasmall size. For a 2-nm QD, most of the atoms comprising it are located on its surface [37]. The lattice distortion caused by the small QD size and high surface-to-volume ratio in this case affect the Raman spectra in a most dramatic way. Phonon confinement in a small QD volume leads to a noticeable broadening of the Raman features because

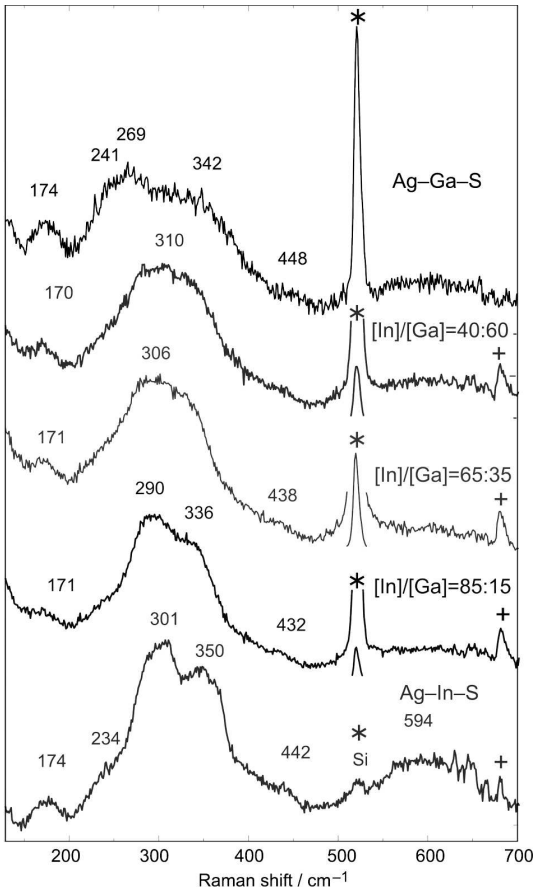

Fig. 4. Raman spectra of Ag–(In,Ga)–S QDs prepared at a [Ag] : [In] : [S] precursor molar ratio and different [In]/[Ga] precursor molar ratios measured using the excitation wavelength λ_{exc} = 488 nm. Asterisks show the silicon substrate peak (521 cm^{-1}). Crosses show methyl viologen peaks

of an increasing contribution of nonzero-wavevector phonons [64]. Surface phonons, the contribution of which to the Raman intensity becomes essentially important for ultrasmall QDs, possess frequencies below those of the LO phonons. This results in the additional smearing of the observed Raman spectra [41, 65]. Note that, for relatively large stoichiometric orthorhombic $AgInS_2$ QDs [56], for which the confinement effects and the surface phonon contribution should be much less pronounced, the observed Raman features are much narrower. It is not surprising that, for small QDs, the size affects the Raman spectra more noticeably than the composition, in particular the [In]/[Ag] ratio for Ag–In–S QDs [39]. This is an important factor that makes Raman spectroscopy in

this particular case a less sensitive tool for compositional characterisation.

One more interesting issue concerns the possible effect of Raman resonance on the measured spectra of the samples under investigation. The closeness of the Raman excitation conditions ($\lambda_{exc} = 488$ nm) to the resonance for the spectra of the Ag–(In,Ga)–S QDs shown in Fig. 4 varied for different chemical compositions due to different bandgap values. However, no drastic differences of the signal-to-noise ratio were observed. Note that an earlier study of Raman scattering for size-selected $AgInS_2$ QDs [34] where the bandgap was varied for the QDs of different sizes, did not reveal any pronounced resonant behavior either. The targeted Raman study of small-size (3–5 nm) non-stoichiometric Ag–(In)–S QDs [41] did not report drastic resonance-related effects, although a redistribution of intensities for $\lambda_{exc} = 633$ nm and a noticeably worse single-to-noise ratio for $\lambda_{exc} = 325$ nm (both quite away from the bandgap value for the major part of the QDs in the polydisperse ensemble) were observed. In our opinion, the absence of pronounced resonance behavior, similarly to our case, can be related to the non-uniformity of the QD size/composition in the sample which always contains sufficient amount of QDs with bandgap energy matching the excitation wavelength, the contribution of which thus dominates in the measured spectrum.

4. Conclusions

Ag–(In,Ga)–S QDs with different [In]/[Ga] ratios are obtained under mild conditions in an exchange reaction from aqueous solutions in the presence of glutathione. Size-selected fractions of the colloidal solutions are separated by the repeated centrifuging with addition of 2-propanol. The QD chemical composition determined by the X-ray photoelectron spectroscopy showed that the [In]/[Ga] ratio in the QDs is noticeably higher than the precursor ratio. The average QD size estimated from the halfwidth of X-ray diffraction peaks for the non-fractioned colloidal solutions is about 2 nm. The broad peak positions in the XRD patterns are in agreement with the tetragonal (chalcopyrite-like) structure of the QDs and exhibit an upward shift with increasing Ga content in the quaternary Ag–(In,Ga)–S QDs. However, for the end-point Ag–(In,Ga)–S QDs, the peak position does not agree with the chalcopyrite-type structure and, as shown earlier [37], testifies for a different (most likely, orthorhombic, rhombohedral, or rocksalt-type) structure.

Optical absorption spectra of the fractionised QDs reveal a distinct shift of the absorption edge toward higher energies with decreasing QD size. A similar, although much less pronounced, shift is observed for the PL maximum position, indicating an increasing Stokes shift for smaller QDs, which is in agreement with the self-trapped exciton mechanism of PL in the I–III–VI QDs. Experimentally measured Raman spectra of the Ag–(In,Ga)–S QDs did not reveal any noticeable compositional variation. This is explained by the ultrasmall QD size, which strongly increases the contribution of surface phonons and confinement effects in the Raman spectra.

Acknowledgement. Y.M. Azhniuk is grateful to the International Office of Chemnitz University of Technology for the financial support of his research stay at the university. Ye.O. Havryliuk is grateful to the Alexander von Humboldt Foundation for the financial support of his research stay at the Chemnitz University of Technology. D.R.T. Zahn and O.V. Selyshchev acknowledge financial support by the Deutsche Forschungsgemeinschaft (DFG project ZA-146/45-1).

1. D. Aldakov, A. Lefrançois, P. Reiss. Ternary and quaternary metal chalcogenide nanocrystals: Synthesis, properties and applications, *J. Mater. Chem. C* **1**, 3756 (2013).
2. J. Kolny-Olesiak, H. Weller. Synthesis and application of colloidal $CuInS_2$ semiconductor nanocrystals, *ACS Appl. Mater. Interfaces* **5**, 12221 (2013).
3. P. Reiss, M. Carriere, C. Lincheneau, L. Vaure, S. Tamang. Synthesis of semiconductor nanocrystals, focusing on nontoxic and earth-abundant materials. *Chem. Rev.* **116**, 10731 (2016).
4. G. Xu, S. Zeng, B. Zhang, M.T. Swihart, K.T. Yong, P.N. Prasad. New generation cadmium-free quantum dots for biophotonics and nanomedicine. *Chem. Rev.* **116**, 12234 (2016).
5. W.M. Girma, M.Z. Fahmi, A. Permadi, M.A. Abate, J.-Y. Chang. Synthetic strategies and biomedical applications of I–III–VI ternary quantum dots. *J. Mater. Chem. B* **5**, 6193 (2017).
6. O. Stroyuk, A. Raevskaya, N. Gaponik. Solar light harvesting with multinary metal chalcogenide nanocrystals. *Chem. Soc. Rev.* **47**, 5354 (2018).
7. Y. Liu, F. Li, H. Huang, B. Mao, Y. Liu, Z. Kang. Optoelectronic and photocatalytic properties of I–III–VI

QDs: Bridging between traditional and emerging new QDs. *J. Semicond.* **41**, 091701 (2020).
8. O. S. Oluwafemi, E. H. M. Sakho, S. Parani, T. C. Lebepe. *Ternary Quantum Dots: Synthesis, Properties, and Applications* (Woodhead Publishing, 2021) [ISBN: 978-0-12-818304-5].
9. K.E. Knowles, K.H. Hartstein, T.B. Kilburn, A. Marchioro, H.D. Nelson, P.J. Whitham, D.R. Gamelin. Luminescent colloidal semiconductor nanocrystals containing copper: Synthesis, photophysics, and applications. *Chem. Rev.* **116**, 10820 (2016).
10. A. Raevskaya, V. Lesnyak, D Haubold, V. Dzhagan, O. Stroyuk, N. Gaponik, D.R.T. Zahn, A. Eychmüller. A fine size selection of brightly luminescent water-soluble Ag–In–S and Ag–In–S/ZnS quantum dots. *J. Phys. Chem. C* **121**, 9032 (2017).
11. O. Stroyuk, A. Raevskaya, F. Spranger, O. Selyshchev, V. Dzhagan, S. Schulze, D.R.T. Zahn, A. Eychmüller. Origin and dynamics of highly efficient broadband photoluminescence of aqueous glutathione-capped size-selected Ag–In–S quantum dots. *J. Phys. Chem. C* **122**, 13648 (2018).
12. B. Zeng, F. Chen, Z. Liu, Z. Guan, X. Li, F, Teng, A. Tang. Seeded-mediated growth of ternary Ag–In–S and quaternary Ag–In–Zn–S nanocrystals from binary Ag_2S seeds and the composition-tunable optical properties. *J. Mater. Chem. C* **7**, 1307 (2019).
13. O. Stroyuk, V. Dzhagan, A. Raevskaya, F. Spranger, N. Gaponik, D.R.T. Zahn. Insights into different photoluminescence mechanisms of binary and ternary aqueous nanocrystals from the temperature dependence: A case study of CdSe and Ag–In–S. *J. Lumin.* **215**, 116630 (2019).
14. O. Stroyuk, O. Raievska, D.R.T. Zahn. Unique luminescent properties of composition-/size-selected aqueous Ag–In–S and core/shell Ag–In–S/ZnS quantum dots. In: *Core/Shell Quantum Dots*. Edited by X. Tong and Z.M. Wang (Springer, 2020), p. 67, [ISBN: 978-3-030-46596-4].
15. M.D. Regulacio, K.Y. Win, S.L. Lo, S.Y. Zhang, X. Zhang, S. Wang, M.Y. Han, Y. Zheng. Aqueous synthesis of highly luminescent $AgInS_2$–ZnS quantum dots and their biological applications. *Nanoscale* **5**, 2322 (2013).
16. L. Jing, S.V. Kershaw, Y. Li, X. Huang, Y. Li, A.L. Rogach, M. Gao. Aqueous based semiconductor nanocrystals. *Chem. Rev.* **116**, 10623 (2016).
17. O. Yarema, M. Yarema, V. Wood. Tuning the composition of multicomponent semiconductor nanocrystals: The case of I–III–VI materials. *Chem. Mater.* **30**, 1446 (2018).
18. M.G. Panthani, T.A. Khan, D.K. Reid, D.J. Hellebusch, M. Rasch, J.A. Maynard, B.A. Korgel. In vivo whole animal fluorescence imaging of a microparticle-based oral vaccine containing $(CuInSe_xS_{2-x})$/ZnS core/shell quantum dots. *Nano Lett.* **13**, 4294 (2013).
19. J.F.L. Lox, Z. Dang, V.M. Dzhagan, D. Spittel, B. Martín-García, I. Moreels, D.R.T. Zahn, V. Lesnyak. Near-infrared Cu–In–Se-based colloidal nanocrystals via cation exchange. *Chem. Mater.* **30**, 2607 (2018).
20. O. Stroyuk, O. Raievska, S. Langner, C. Kupfer, A. Barabash, D. Solonenko, Y, Azhniuk, J. Hauch, A. Osvet, M. Batentschuk, D.R.T. Zahn, C.J. Brabec. High-throughput robotic synthesis and photoluminescence characterization of aqueous multinary copper-silver indium chalcogenide quantum dots. *Particle and Particle Systems Characterization* **2021**, 202100169 (2021).
21. O. Raievska, O. Stroyuk, Y. Azhniuk, D. Solonenko, A. Barabash, C.J. Brabec, D.R.T. Zahn. Composition-dependent optical band bowing, vibrational and photochemical behavior of aqueous glutathione-capped (Cu,Ag)–In–S quantum dots. *J. Chem. Phys. C* **124**, 19375 (2020).
22. O. Stroyuk, O. Raievska, D. Solonenko, C. Kupfer, A. Osvet, M. Batentschuk, C.J. Brabec, D.R.T. Zahn. Spontaneous alloying of ultrasmall nonstoichiometric Ag–In–S and Cu–In–S quantum dots in aqueous colloidal solutions. *RSC Adv.* **11**, 21145 (2021).
23. T. Uematsu, T. Doi, T. Torimoto, S. Kuwabata. Preparation of luminescent $AgInS_2$–$AgGaS_2$ solid solution nanoparticles and their optical properties. *J. Phys. Chem. Lett.* **1**, 3283 (2010).
24. S. Maeda, T. Uematsu, T. Doi, J. Tokuda, T. Fujita, T. Torimoto, S. Long-term optical properties of ZnS–$AgInS_2$ and $AgInS_2$–$AgGaS_2$ solid-solution semiconductor nanoparticles dispersed in polymer matrices. *Electrochem.* **79**, 813 (2011).
25. N. Liang, Q. He, S. Huang, M. Wang, W. Chen, M. Xu, Y. Yuan, J. Zai, N. Fang, X. Qian. $AgIn_xGa_{1-x}S_2$ solid solution nanocrystals: Synthesis, band gap tuning and photocatalytic activity. *Cryst. Eng. Comm.* **16**, 10123 (2014).
26. T. Kameyama, C. Miyamae, D.K. Sharma, S. Hirata, T. Yamamoto, M. Vacha, S. Kuwabata, T. Torimoto. Wavelength-tunable band-edge photoluminescence of non-stoichiometric Ag–In–S nanoparticles via Ga^{3+} doping. *ACS Appl. Mater. Interfaces* **10**, 42844 (2018).
27. M. Ichimiya, T. Kameyama, T. Torimoto, T. Uematsu, S. Kuwabata, A. Ashida. Temperature dependences of photoluminescence intensities observed from AgInGaS and AgInGaS/GaS_x core–shell nanoparticles. *J. Nanophoton.* **14**, 016010 (2020).
28. W. Hoisang, T. Uematsu, T. Torimoto, S. Kuwabata. Luminescent quaternary $Ag(In_xGa_{1ıx})S_2/GaS_y$ core/shell quantum dots prepared using dithiocarbamate compounds and photoluminescence recovery via post treatment. *Inorg. Chem.* **60**, 13101 (2021).
29. W. Hoisang, T. Uematsu, T. Torimoto, S. Kuwabata. Surface ligand chemistry on quaternary $Ag(In_xGa_{1-x})S_2$/GaS_y semiconductor quantum dots for improving photoluminescence properties. *Nanoscale Adv.* **4**, 849 (2022).
30. J.H. Kim, B.Y. Kim, E.P. Jang, S.Y. Yoon, K.H. Kim, Y.R. Do, H. Yang. Synthesis of widely emission-tunable Ag–Ga–S and its quaternary derivative quantum dots. *Chem. Eng. J.* **347**, 791 (2018).vspace*-0.3mm
31. T. Bai, X. Wang, Y. Dong, Z. Shi, S. Feng. One-pot synthesis of high-quality $AgGaS_2$/ZnS-based photoluminescent

nanocrystals with widely tunable band gap. *Inorg. Chem.* **59**, 5975 (2020).
32. J. Song, Y. Zhang, Y. Dai, J. Hu, L. Zhu, X. Xu, Y. Yu, H. Li, B. Yao, H. Zhou. Polyelectrolyte-mediated nontoxic $AgGa_xIn_{1-x}S_2$ QDs/low-density lipoprotein nanoprobe for selective 3D fluorescence imaging of cancer stem cells. *ACS Appl. Mater. Interfaces* **11**, 9884 (2019).
33. A. Raevskaya, O. Rozovik, A. Novikova, O. Selyshchev, O. Stroyuk, V. Dzhagan, I. Goryacheva, N. Gaponik, D.R.T. Zahn, A. Eychmüller. Luminescence and photoelectrochemical properties of size-selected aqueous copper-doped Ag–In–S quantum dots. *RSC Adv.* **8**, 7550 (2018).
34. B.V. Lopushanska, Y.M. Azhniuk, I.P. Studenyak, V.V. Lopushansky, A.V. Gomonnai, D.R.T. Zahn. Optical characterization of colloidal $AgInS_2$ quantum dots synthesized from aqueous solutions. *J. Nano- and Electron. Phys.* **14**, 04010 (2022).
35. A. Raevskaya, O. Rosovik, A. Kozytskiy, O. Stroyuk, V. Dzhagan, D.R.T. Zahn. Non-stoichiometric Cu–In–S/ZnS nanoparticles produced in aqueous solutions as light harvesters for liquid-junction photoelectrochemical solar cells. *RSC Adv.* **6**, 100145 (2016).
36. Y.M. Azhniuk, Ye.O. Havryliuk, B.V. Lopushanska, V.V. Lopushansky, A.V. Gomonnai, D.R.T. Zahn. Structural and optical characterisation of size-selected glutathione-capped colloidal Cu–In–S quantum dots. *Ukr. J. Phys.* **68**, 190 (2023).
37. Y. Azhniuk, B. Lopushanska, O. Selyshchev, Y. Havryliuk, A. Pogodin, O. Kokhan, A. Ehm, V. Lopushansky, I. Studenyak, D.R.T. Zahn. Synthesis and optical properties of Ag–Ga–S quantum dots. *Phys. Status Solidi B* **259**, 2100349 (2022).
38. B.V. Lopushanska, Y.M. Azhniuk, V.V. Lopushansky, S.B. Molnar, I.P. Studenyak, O.V. Selyshchev, D.R.T. Zahn. Synthesis from aqueous solutions and optical properties of Ag–In–S quantum dots. *Appl. Nanosci.* **10**, 4909 (2020).
39. B.V. Lopushanska, Y.M. Azhniuk, D. Solonenko, V.V. Lopushansky, I.P. Studenyak, D.R.T. Zahn. Structural and optical study of glutathione-capped Ag–In–S nanocrystals. *Molec. Cryst. Liquid. Cryst.* **717**, 98 (2021).
40. D.E. Nam, W.S. Song, H. Yang. Noninjection, one-pot synthesis of Cu-deficient $CuInS_2$/ZnS core/shell quantum dots and their fluorescent properties. *J. Colloid Interface Sci.* **361**, 491 (2011).
41. V. Dzhagan, O. Selyshchev, O. Raievska, O. Stroyuk, L. Hertling, N. Mazur, M.Y. Valakh, D.R.T. Zahn. Phonon spectra of strongly luminescent nonstoichiometric Ag–In–S, Cu–In–S, and Hg–In–S nanocrystals of small size. *J. Phys. Chem. C* **124**, 15511 (2020).
42. F. Huang, J. Zhou, J. Xu, Y. Wang. Formation of $AgGaS_2$ nano-pyramids from Ag_2S nanospheres through intermediate Ag_2S–$AgGaS_2$ heterostructures and $AgGaS_2$ sensitized Mn^{2+} emission. *Nanoscale* **6**, 2340 (2014).
43. C. Lin, L. Calvez, B. Bureau, H. Tao, M. Allix, Z. Hao, V. Seznec, X. Zhang, X. Zhao. Econd-order optical nonlinearity and ionic conductivity of nanocrystalline GeS_2–Ga_2S_3–LiI glass-ceramics with improved thermo-mechanical properties. *Phys. Chem. Chem. Phys.* **12**, 3780 (2010).
44. L. Yuan, S. Lu, F. Yang, Y. Wang, Y. Jia, M. Kadhim, Y. Yu, Y. Zhang, Y. Zhao. A facile room-temperature synthesis of three-dimensional coral-like Ag_2S nanostructure with enhanced photocatalytic activity. *J. Mater. Sci.* **54**, 3174 (2019).
45. T. Ogawa, T. Kuzuya, Y. Hamanaka, K. Sumiyama. Synthesis of Ag–In binary sulfide nanoparticles – structural tuning and their photoluminescence properties. *J. Mater. Chem.* **20**, 2226 (2010).
46. S.P. Hong, H.K. Park, J.H. Oh, H. Yang, Y.R. Do. Comparisons of the structural and optical properties of o-$AgInS_2$, t-$AgInS_2$, and c-$AgIn_5S_8$ nanocrystals and their solid-solution nanocrystals with ZnS. *J. Mater. Chem.* **22**, 18939 (2012).
47. T. Torimoto, M. Tada, M. Dai, T. Kameyama, S. Suzuki, S. Kuwabata. Tunable photoelectrochemical properties of chalcopyrite $AgInS_2$ nanoparticles size-controlled with a photoetching technique. *J. Phys. Chem. C* **116**, 21895 (2012).
48. E. Soheyli, D. Azad, R. Sahraei, A.A. Hatamnia, A. Rostamzad, M. Alinazari. Synthesis and optimization of emission characteristics of water-dispersible Ag–In–S quantum dots and their bactericidal activity. *Coll. Surf. B: Biointerfaces* **182**, 110389 (2019).
49. A. Delices, D. Moodelly, C. Hurot, Y. Hou, W.L. Ling, C. Saint-Pierre, D. Gasparutto, G. Nogues, P. Reiss, K. Kheng. Aqueous synthesis of DNA-functionalized near-infrared $AgInS_2$/ZnS core/shell quantum dots. *ACS Appl. Mater.* **12**, 44026 (2020).
50. R.S. Roth, H.S. Parker, W.S. Brower. Comments on the system Ag_2S–In_2S_3. *Mater. Res. Bull.* **8**, 333 (1973).
51. K. Yoshino, A. Kinoshita, K. Nomoto, T. Kakeno, S. Seto, Y. Akaki, T. Ikari. Pressure dependence of $AgInS_2$ crystals grown by hot-press method. *Phys. Status Solidi C* **3**, 2648 (2006).
52. K.J. Range, B. Lindenberg, M. Keubler, R. Leeb, A. Weiss. Über den Einfluß kinetischer Hemmungen auf die Hochdruck um wandlungen des $AgInS_2$. *Z. Naturforsch. B* **24**, 1651 (1969).
53. K.J. Range, M. Keubler, A. Weiss. Eine Hochdruckmodifikation des $AgInS_2$ mit α-$NaFeO_2$-Struktur. *Z. Naturforsch. B* **21**, 1060 (1969).
54. A.L. Rogach, A. Kornowski, M. Gao, A. Eychmüller, H. Weller. Synthesis and characterization of a size series of extremely small thiol-stabilized CdSe nanocrystals. *J. Phys. Chem. B* **103**, 3065 (1999).
55. O. Stroyuk, F. Weigert, A. Raevskaya, F. Spranger, C. Würth, U. Resch-Genger, N. Gaponik, D.R.T. Zahn. Inherently broadband photoluminescence in Ag–In–S/ZnS quantum dots observed in ensemble and single-particle studies. *J. Phys. Chem. C* **123**, 2632 (2019).
56. F.Y. Lee, K.Y. Yang, C.H. Li, T.R. Lee, T.C. Lee. Electrochemical properties of an $AgInS_2$ photoanode prepared us-

ing ultrasonic-assisted chemical bath deposition. *RSC Adv.* **4**, 35215 (2014).
57. B. Cichy, R.M. Rich, A. Olejniczak, Z. Gryczynski, W. Strek. Two blinking mechanisms in highly confined $AgInS_2$ and $AgInS_2$/ZnS quantum dots evaluated by single particle spectroscopy. *Nanoscale* **8**, 4151 (2016).
58. A. Hirase, Y. Hamanaka, T. Kuzuya. Ligand-induced luminescence transformation in $AgInS_2$ nanoparticles: From defect emission to band-edge emission. *J. Phys. Chem. Lett.* **11**, 3969 (2020).
59. V. Dzhagan, A.P. Litvinchuk, M.Y. Valakh, D.R.T. Zahn. Phonon Raman spectroscopy of nanocrystalline multinary chalcogenides as a probe of complex lattice structures. *J. Phys.: Condens. Matter* **35**, 103001 (2023).
60. Y.M. Azhniuk, A.V. Gomonnai, D. Solonenko, V. Loya, I. Voynarovych, B. Lopushanska, I. Roman, V. Lopushansky, D.R.T. Zahn. Raman and X-ray diffraction study of Ag–In–S polycrystals, films, and nanoparticles. *J. Mater. Res.* **38**, 2239 (2023).
61. F. W. Ohrendorf, H. Haeuseler. Lattice dynamics of chalcopyrite type compounds. Part I. Vibrational frequencies. *Cryst. Res. Technol.* **34**, 339 (1999).
62. I.H. Choi, S.H. Eom, P.Y. Yu. The optical and vibrational properties of the quaternary chalcopyrite semiconductor alloy $Ag_xCu_{1-x}GaS_2$. *J. Appl. Phys.* **87**, 3815 (2000).
63. Y.M. Azhniuk, Y.I. Hutych, V.V. Lopushansky, M.V. Prymak, A.V. Gomonnai, D.R.T. Zahn. Chemical composition of matrix-embedded ternary II–VI nanocrystals derived from first- and second-order Raman spectra. *J. Phys. Chem. Solids* **99**, 66 (2016).
64. V.M. Dzhagan, Y.M. Azhniuk, A.G. Milekhin, D.R.T. Zahn. Vibrational spectroscopy of compound semiconductor nanocrystals. *J. Phys. D* **51**, 503001 (2018).
65. M.Ya. Valakh, V.M. Dzhagan, A.E. Raevskaya, S.Ya. Kuchmiy. Optical investigations of ultra-small colloidal nanoparticles and heteronanoparticles based on II–VI semiconductors. *Ukr. J. Phys.* **56**, 1080 (2011).

Received 10.04.23

Ю.М. Ажнюк, О.В. Селищев, Є.О. Гаврилюк, Б.В. Лопушанська, А. Ем, В.В. Лопушанський, А.В. Гомоннай, І.П. Студеняк, Д.Р.Т. Цан

ВКРИТІ ГЛУТАТІОНОМ ЧОТИРИКОМПОНЕНТНІ КВАНТОВІ ТОЧКИ Ag–(In,Ga)–S, ОТРИМАНІ КОЛОЇДНИМ СИНТЕЗОМ У ВОДНИХ РОЗЧИНАХ

Квантові точки (КТ) Ag–(In,Ga)–S отримано колоїдним синтезом за помірних умов у водних розчинах з різним співвідношенням прекурсорів [In]/[Ga] у присутності глутатіону як ліганда. Колоїдні розчини розділено на розмірні фракції повторним центрифугуванням з додаванням 2-пропанолу. Хімічний склад КТ, визначений з даних рентгенівської фотоелектронної спектроскопії, вказує на помітно вищий вміст In у порівнянні зі співвідношенням прекурсорів. Розмір КТ, визначений з напівширини піків дифракції рентгенівських променів для нефракціонованих колоїдних розчинів, приблизно дорівнює 2 нм. Синтезовані КТ характеризуються зміщенням краю поглинання і положення максимуму фотолюмінесценції в бік вищих енергій зі зменшенням розміру КТ. В експериментально виміряних спектрах раманівського розсіювання КТ Ag–(In,Ga)–S помітний вплив факторів, пов'язаних з розміром КТ.

Ключові слова: колоїдний синтез, квантові точки, рентгенівська фотоелектронна спектроскопія, рентгенівська дифракція, оптичне поглинання, фотолюмінесценція, раманівська спектроскопія.